Stability and electronic structure of two-dimensional allotropes of group-IV materials

Filipe Matusalem,[1,*] Marcelo Marques,[1] Lara K. Teles,[1] and Friedhelm Bechstedt[2]

[1]*Grupo de materiais semicondutores e nanotecnologia (GMSN), Instituto Tecnológico de Aeronáutica (ITA), 12228-900 São José dos Campos/SP, Brasil*

[2]*Institut für Festkörpertheorie und -optik, Friedrich-Schiller-Universität, Max-Wien-Platz 1, D-07743 Jena, Germany*

(Received 5 May 2015; revised manuscript received 9 July 2015; published 29 July 2015)

We study six different two-dimensional (2D) allotropes of carbon, silicon, germanium, and tin by means of the *ab initio* density functional theory for the ground state and approximate methods to calculate their electronic structures, including quasiparticle effects. Four of the investigated allotropes are based on dumbbell geometries, one on a kagome lattice, and one on the graphenelike hexagonal structure for comparison. Concerning carbon, our calculations of the cohesive energies clearly show that the hexagonal structure (graphene) is most stable. However, in the case of Si and Ge, the dumbbell structures, particularly the large honeycomb dumbbell (LHD) geometries, are energetically favored compared to the sp^2/sp^3-bonded hexagonal lattice (i.e., silicene and germanene). The main reason for this is the opening of a band gap in the honeycomb dumbbell arrangements. The LHD sheet crystals represent indirect semiconductors with a $K \rightarrow \Gamma$ gap of about 0.5 eV. In the Sn case we predict the MoS_2-like symmetry to be more stable, in contrast to the stanene and LHD geometries predicted in literature. Our results for freestanding group-IV layers shine new light on recent experimental studies of group-IV overlayers on various substrates.

DOI: 10.1103/PhysRevB.92.045436 PACS number(s): 68.55.ag, 71.15.Nc, 71.15.Qe, 73.22.−f

I. INTRODUCTION

Recently, after the rediscovery and synthesis of graphene [1–5] and inspired by its exotic structural, topological, optical, and electronic properties [6–11], a great interest in two-dimensional (2D) materials has emerged. Naturally, the other group-IV elements have been considered as candidates to have a graphenelike hexagonal, honeycomb structure with similar exceptional properties. Indeed, corresponding 2D structures for other group-IV elements have been predicted and studied theoretically, namely, silicene (Si-based), germanene (Ge-based), and stanene (or tinene) (Sn-based) [12–18]. Different from graphene, in the sheet the silicon atoms are buckled, which makes an electronic system with a partial sp^3 hybridization. The most stable configuration is, however, the low-buckled one [12]. Also, germanene and stanene have a buckled structure [12,14–16,19]. Experimentally, the 2D honeycomb structure of silicon has been claimed to be deposited mainly on Ag(111) substrates [20–22]. More recently, experimental evidence of germanene, grown by molecular beam epitaxy using a gold (111) surface as a substrate, has been found [23]. The fully hydrogenated germanene sheet, germanane, has been discovered previously [24].

In order to explain some characteristics of silicene, grown on Ag(111) surfaces, some modifications of this graphenelike structure have been proposed. It has been shown that the addition of Si adatoms to pristine silicene results in the formation of a dumbbell structure with a lower total energy per atom [25,26]. The dumbbell structure is obtained by addition of an extra silicon atom adsorbed at the top site of the silicene. This Si adatom pushes down the Si atom underneath to form a dumbbell-like structure with 3 + 1 coordination [25]. A 2D supercell, which fits to a certain substrate, can be constructed in such a way to increase or decrease the density of dumbbell units.

For silicene grown on Ag(111) surfaces, frequently a periodicity of $\sqrt{3} \times \sqrt{3}$ with respect to the 1×1 silicene lattice is observed [27–29]. To explain the $\sqrt{3} \times \sqrt{3}$ translational symmetry and honeycomb images in the scanning tunneling microscopy (STM), Cahangirov *et al.* [30] proposed an adsorbed silicene with one dumbbell unit [trigonal dumbbell (TD) silicene] or two dumbbell units [honeycomb dumbbell (HD) silicene] (see Fig. 1). Both structures have been found to be more stable than freestanding, graphenelike silicene. However, although TD and HD silicene can match the lattice parameter of a silicene overlayer on Ag(111), these two structures as freestanding objects are less stable than the large honeycomb dumbbell (LHD) silicene, which is a 2×2 silicene with two dumbbell units [30] (see Fig. 1). This LHD phase was also studied for stanene, the graphenelike allotrope of tin, which should be a quantum spin Hall insulator [17,31].

Another possible allotrope for 2D silicon, which is a phase bearing structural resemblance to a single MoS_2 (i.e., triple atomic) layer (see Fig. 1), should have a lower total energy than low-buckled pristine silicene and be, at least, metastable in terms of its phonon dispersion relations [32]. In principle, because of the same atoms the bonding elements of this geometry can be also interpreted as dumbbells. Very recently a three-dimensional (3D) elemental carbon kagome lattice (KL) made of only fourfold-coordinated carbon atoms and 60° bond angles in triangles has been proposed [33,34], as well as 2D deformed kagome lattices with hexagonal symmetry [35] (see Fig. 1).

There are several suggestions for possible 2D sheet crystals. Details of their atomic geometries and bonding behavior, but especially their electronic structures along the group-IV elements in the periodic table, are not known. Chemical trends and their violation require clarification. In this work we make a comparative *ab initio* study for the group-IV elements carbon, silicon, germanium, and tin in six 2D allotropes: graphenelike (HEX), LHD, TD, HD, MoS_2-like (MoS_2), and KL geometries. The electronic band structures

*filipematus@gmail.com, gmsn@ita.br

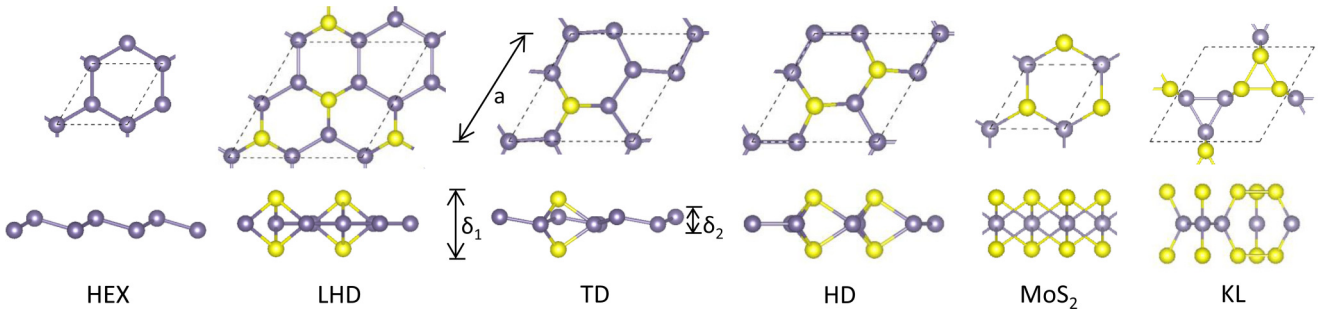

FIG. 1. (Color online) Top and side view of the six 2D bonding geometries with hexagonal or trigonal symmetry HEX, LHD, TD, HD, MoS_2, and KL studied in this work. The lattice parameters a, δ_1, and δ_2 indicate the unit cell size and the largest and smallest layer buckling, respectively. Group-IV atoms out of the plane are indicated by yellow spheres.

of all nonmetallic geometries are investigated, including approximate quasiparticle corrections. The article is organized as follows: In Sec. II we describe the methods adopted in our calculations. In Sec. III we present and discuss the results. Finally, in Sec. IV we briefly summarize the paper.

II. THEORETICAL AND NUMERICAL METHODS

We perform density functional theory (DFT) calculations employing a semilocal approach for exchange and correlation within the generalized-gradient approximation (GGA). The GGA is employed to determine the theoretical lattice parameters and relaxed positions of ions. The Kohn-Sham equations are solved self-consistently within the projector augmented wave (PAW) [36,37] scheme as implemented in the Vienna Ab Initio Simulation Package (VASP) [38–40]. For the plane-wave expansion of the electronic wave functions we use an energy cutoff of 400, 245, 174, and 103 eV for carbon, silicon, germanium, and tin, respectively.

In order to simulate the 2D structures with different translational and point group symmetries we apply the superlattice method. The sheet crystals are repeated in vertical direction. The distance between the 2D sheets in the perpendicular direction is taken at least 20 Å. The Brillouin zone (BZ) was sampled with $16 \times 16 \times 1$, $12 \times 12 \times 1$, $36 \times 36 \times 1$, $20 \times 20 \times 1$, $28 \times 28 \times 1$, and $20 \times 20 \times 1$ grids of k points, for HEX, LHD, TD, HD, MoS_2, and KL lattices, respectively, in the Monkhorst-Pack scheme [41]. The structure optimization is done by bringing the atomic forces to values smaller than 1 meV/Å. The total energies resulting for the optimized geometries are used to discuss the energetic stability of the 2D allotropes. Cohesive energies are obtained by the difference between the total energy per atom of such a structure and that of a free atom. The total energy of the free atom is computed using repeated supercells with an edge length of 20 Å. For the free atom spin polarization is taken into account.

The resulting eigenvalues of the Kohn-Sham equations do not account for the excitation aspect, that excited electrons and holes become quasiparticles [42]. Consequently, the fundamental gaps of semiconductors and insulators, in general, the distances of occupied and empty energy bands, are underestimated [42,43]. In order to simulate the quasiparticle shifts we apply the GGA-1/2 approach [44,45] for the group-IV allotropes which have a band gap, namely, the LHD and HD geometries. This method is a simple, low time consuming, and parameter-free procedure to compute excitation energies. It calculates the self-energy as the quantum mechanical average of a "self-energy potential," V_S, which is added to the local part of the pseudopotential or to the $-2Z/r$ part of the all-electron potential. A trimming is performed to prevent the self-energy potential from extending to neighboring atoms. This trimming is made by means of a step function with a parameter CUT, which is determined variationally, maximizing the band gap, as explained in Refs. [44,45]. Then the excitation of an electron from the valence to the conduction band is described as

$$\text{True Band Gap} = \text{Kohn-Sham Band Gap} + S_v - S_c, \quad (1)$$

where S_v and S_c are the self-energies caused by the localization of the excitation of the hole in the valence band (VB) and the electron in the conduction band (CB), respectively.

Usually, the potential V_S is applied to the states at the top of the valence band, in most cases the valence p orbital. The self-energy of the electron in a CB is neglected, apart from germanium. In this case we first include the self-energy potential for the p valence states and maximize the gap with respect to CUT. The CUT parameter characterizes the extent of the hole excitation. Then, with the optimized CUT we also include the self-energy potential for s conduction states. For bulk diamond Ge a new maximization results in an indirect gap of $E_g^{\Gamma-L} = 0.86$ eV, near to the experimental value $E_g^{\Gamma-L} = 0.74$ eV (at $T = 0$ K) [46], when considering the experimental lattice parameter. So, for all germanium-based geometries, we also include the self-energy for the electron in the CB.

In a second approach to electronic excitations, a hybrid functional description of exchange and correlation is used for comparison purposes. It accounts for the most important spatial nonlocality of the exchange-correlation self-energy. Explicit calculations are done using the Heyd-Scuseria-Ernzerhof hybrid functional (HSE06) [47,48].

III. RESULTS AND DISCUSSION

A. Geometry and energetics

We performed DFT-GGA calculations for the 2D allotropes of carbon, silicon, germanium, and tin. Six different geometries shown in Fig. 1, HEX, LHD, TD, HD, MoS_2, and KL, have been investigated. The most important structural parameters are given in Table I. The resulting cohesive energies are listed in Table II. For comparison, the corresponding values obtained for the three-dimensional (3D) diamond structure of the

TABLE I. Calculated lattice parameter and buckling height for the 2D allotropes of group-IV materials. Except for KL, the lattice constants are normalized to an equivalent lattice of a 2×2 HEX structure. The second-nearest-neighbor distance is given in the diamond case. For comparison (experimental) other [theoretical GGA] results are presented.

	Lattice parameter (Å)						
	HEX	LHD	TD	HD	MoS_2	KL	Diamond
C	4.94(4.92) [8]	4.88	4.90	4.97	5.02	4.56	5.05(5.04) [46]
Si	7.74(7.38) [29]	7.43[7.67] [30]	7.55[7.35] [30]	7.37[7.36] [30]	7.20[7.28] [32]	6.84	7.74(7.68) [46]
Ge	8.12(8.31) [53]	7.88	7.99	7.82	7.70[7.80] [32]	7.24	8.18(8.00) [46]
Sn	9.34	9.05[9.05] [31]	9.19	8.94	6.58	8.23	9.41(9.18) [46]
	δ_1 (Å)						δ_2 (Å)
	HEX	LHD	TD	HD	MoS_2	KL	TD
C	0.00	1.59	1.58	1.59	1.63	2.32	0.00
Si	0.45	2.71	2.76	2.66	2.63	3.93	0.01
Ge	0.69	2.96	2.97	2.90	2.84	4.24	0.44
Sn	0.85	3.42	3.38	3.34	5.44	4.90	0.61

group-IV elements are also given. The latter values illustrate the quality of the DFT-GGA treatment. The experimental lattice constants of the diamond structure are 3.57 (C), 5.43 (Si), 5.66 (Ge), and 6.49 (Sn) Å [46]. Along the row C→Sn the theoretical values in Table I are increasingly slightly larger than the experimental ones, indicating the underbinding tendency of the GGA [42]. The cohesive energies 7.37 (C), 4.63 (Si), 3.85 (Ge), and 3.14 (Sn) eV/atom measured for diamond crystals [46] are, however, close to the computed energies in Table II.

Whereas the bulk 3D diamond crystals consist only of fourfold-coordinated group-IV atoms with complete sp^3 bonding, this behavior is modified in the 2D allotropes. The low-buckled pristine HEX geometries are built by threefold-coordinated atoms with mixed sp^2/sp^3 bonding behavior (Fig. 1). The tendency from sp^2 to sp^3 is increased along the increasing bond length, as depicted by the layer buckling δ_1 in Table I. The point group associated with its full space group is D_{6h} (C) or D_{3d} (Si, Ge, Sn). Adsorption of the same group-IV atoms on a monolayer honeycomb structure tends to the formation of dumbbells with a $3+1$ coordination of the atoms. The additional atoms form dangling bonds with almost sp^3 hybridization, which bond to the other atoms and stabilize a more complex 2D structure. The number of adatoms which form three bonds to the monolayer determine the size of the unit cell (see Fig. 1). The resulting dumbbells, one (TD) or two (HD) per nonprimitive $\sqrt{3} \times \sqrt{3}$ unit cell or two (LHD) per nonprimitive 2×2 cell of the underlying honeycomb geometry, determine the stability of the 2D allotrope. The LHD structure has a high symmetry with the point group D_{6h} (independent of the group-IV atom), despite the increased number of 10 atoms in the unit cell. The symmetry is reduced for HD with D_{3h} (independent of the group-IV atom) and TD with D_{3h} (C) or C_{3v} (Si, Ge, Sn). A periodic arrangement of dumbbells may form a geometry similar to the triple layer of MoS_2 (see Fig. 1). In such a structure the central group-IV atom is sixfold coordinated. The other two atoms per 1×1 unit cell realize their bonds by "nematic" orbitals originating from sp^2 orbitals [27]. Its point group is D_{3h} (independent of the group-IV element). Finally, the last image in Fig. 1 represents a two-dimensional KL, or a basket-weave lattice [49]. It consists of zigzag chains of interlaced triangles of group-IV atoms together with some 60° bonds [50]. Its point group is also D_{3h} (independent of the group-IV atom). All allotropes possess a high hexagonal or trigonal point-group symmetry.

In Table I the calculated lattice constants (respective lattice parameters related to the 2×2 case) and buckling heights are listed for the six considered 2D allotropes of C, Si, Ge, and Sn. For the HEX structure of carbon, i.e., graphene, we calculate a lattice constant of 2.47 Å, in excellent agreement with the experimental value of 2.46 Å [8] and theoretical value of 2.45 Å using a local [51] or semilocal spin-polarized [52] functional for exchange and correlation.

The structural parameters listed in Table I agree widely with other theoretical results [12,13,15,16,19,26]. For silicon, in the HEX structure, i.e., silicene, we calculate a lattice constant of 3.87 Å and a Si-Si distance of 2.28 Å, in good agreement with experimental values of 3.69 Å [29] and 2.2 Å [20,21], respectively. Also, our results are in agreement with the theoretical values of Cahangirov *et al.* [12] for lattice constant, 3.87 Å; Si-Si distance, 2.25 Å; and buckling height, 0.45 Å. For LHD, TD, and HD structures we obtain lattice parameters of 7.43 Å (or 6.23 Å in terms of the length corresponding to $\sqrt{3} \times \sqrt{3}$ cell), 6.52 Å, and 6.39 Å, respectively. These

TABLE II. Cohesive energy for the 2D allotropes of group-IV materials. Values in parenthesis are theoretical results from Ref. [30].

	Cohesive energy (eV/atom)						
	Diamond	HEX	LHD	TD	HD	MoS_2	KL
C	7.77(7.35) [46]	7.90	6.94	6.96	6.07	5.22	6.59
Si	4.54(4.63) [46]	3.89(3.85)	4.10(4.16)	3.94(4.01)	3.95(4.02)	3.90	3.70
Ge	3.67(3.85) [46]	3.19	3.35	3.22	3.30	3.29	3.09
Sn	3.12	2.68	2.86	2.74	2.84	2.91	2.11

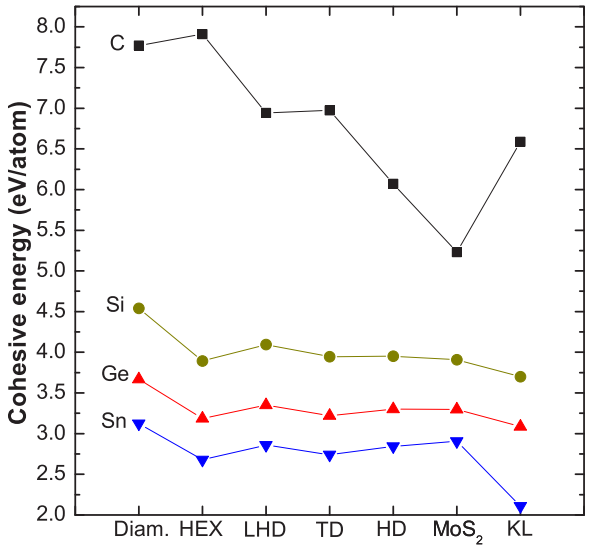

FIG. 2. (Color online) Cohesive energies of group-IV materials of different 2D allotropes compared with bulk diamond geometries.

values are in good agreement with previous results [30], whose values were 6.43 Å, 6.52 Å, and 6.38 Å for LHD, TD, and HD, respectively. For silicon in a MoS_2-like structure we obtain a lattice parameter of 3.60 Å and a buckling height of 2.63 Å. Both values are in excellent agreement with work of Gimbert *et al.* [32], which found 3.64 and 2.63 Å, respectively.

For germanium, in HEX structure, i.e., germanene, we calculate, a lattice parameter of 4.06 Å and a Ge-Ge distance of 2.44 Å. The latter value is somewhat larger than the experimental value of 2.21 Å for Ge-Ge distance on Au(111) substrates [23]. Our results are in agreement with theoretical ones of Cahangirov *et al.* [12] for lattice constant, 4.15 Å, Ge-Ge distance, 2.38 Å, and buckling height, 0.64 Å. For germanium in MoS_2-like structure we obtain a lattice parameter of 3.86 Å, and a buckling height 2.84 Å. Both are in excellent agreement with work of Gimbert *et al.* [32], which are 3.90 Å and 2.88 Å, respectively.

For tin, our structural parameters are in excellent agreement with the result of Tang *et al.* [31], who obtained a lattice parameter of 9.05 Å and a buckling height δ_1 of 3.41 Å for the LHD structure.

In Table II we list the cohesive energies per atom for diamond crystals and 2D allotropes of group-IV elements. The chemical trends of the cohesive energies are shown in Fig. 2 for the different structures. The 3D diamond structure is the most stable geometry for all atoms, except for carbon (at least in the framework of DFT-GGA), which has a higher cohesive energy for graphene. The other 2D structures based on carbon are significantly less stable compared to graphene, in agreement with the preference of sp^2 bonding for C atoms. Among the 2D allotropes of Si and Ge, the LHD structure is somewhat more stable. The preference of Si(Ge) for the LHD structure versus silicene(germanene) by 0.21(0.16) eV per atom in Fig. 2 and Table II confirms the finding. For Sn, the MoS_2 structure is 0.05 eV per atom more stable than the LHD structure, which is 0.18 eV per atom more stable than stanene, the commonly favored 2D tin geometry. In general, the MoS_2-like structures are more stable than silicene, germanene, and stanene, in agreement with other theoretical findings for Si and Ge [32]. Also, for the MoS_2 geometry, the energy of the system as a function of δ_1 exhibits two distinct minima. The global minimum for Sn is given by the large δ_1, while for Ge and Si it occurs at a small δ_1 (see Table I). Therefore the differences between Si or Ge and Sn for the MoS_2 geometry can be related to the fact that a larger δ_1 parameter for Sn permits a larger density of dumbbells, in contrast to Si or Ge.

The 2D KL structure for carbon has a intermediate cohesive energy among the 2D structures, with a value slightly smaller than that of LHD or TD. In Fig. 2 for silicon and germanium the 2D KL is shown to be slightly smaller in energy than the other 2D structures. This result is in contrast to findings for 3D KL structures which possess cohesive energies only slightly smaller than the Si and Ge diamond values [34]. On the other hand, for tin the 2D KL lattice can be clearly excluded from possible freestanding 2D geometries due to its low cohesive energy.

B. Electronic structure

The electronic band structures obtained within GGA and GGA-1/2 are displayed for the four 2D allotropes HEX, LHD, HD, and KL in Fig. 3. The complete band structures of TD and MoS_2 are not plotted because of the strong metallic character of these allotropes. For the metallic or zero-gap semiconductor structures shown in Fig. 3, we used, for GGA-1/2 calculations, a CUT parameter obtained as an average between those calculated for the 2D allotropes which have a gap, namely, LHD and HD. For carbon the CUT parameter used is the one obtained for LHD phase, since HD is metallic. For orientation and energy alignment, also the bands of the semiconducting diamond structure are given.

Three different CUT values are obtained for each atom (six for Ge), one for each structure, 3D diamond and 2D LHD or HD. The CUT parameter value is influenced by the environment where the atom is placed, i.e., for different structures an atom can have different CUT values. This is in agreement with the screening reaction underlying the formation of quasiparticles during excitation. The CUT values vary only slightly from allotrope to allotrope, highlighting their almost transferability to different atomic geometries. The CUT parameters are only somewhat larger for the 2D systems compared to the 3D diamond value. However, the CUT parameters significantly vary with the element. A pronounced increase is visible along the row C→Si→Ge→Sn. This increase is strictly related to the bond lengths in the systems. For instance, in the diamond case, expressed in units of the lattice constant from Table I, the CUT value is almost constant with 0.47 (C), 0.47 (Si), 0.50 (Ge), and 0.50 (Sn).

The corresponding fundamental energy gaps are given in Table III within GGA, GGA-1/2, and HSE quality. The metallic or zero-gap semiconductor character of the other 2D allotropes are obvious from their band structures obtained within GGA (not shown in Fig. 3 for TD and MoS_2). The approximate quasiparticle GGA-1/2 and HSE band structures of the gapped systems are rather similar. This is clearly confirmed by the size of the energy gaps in Table III. For that reason only GGA-1/2 and not HSE bands are compared

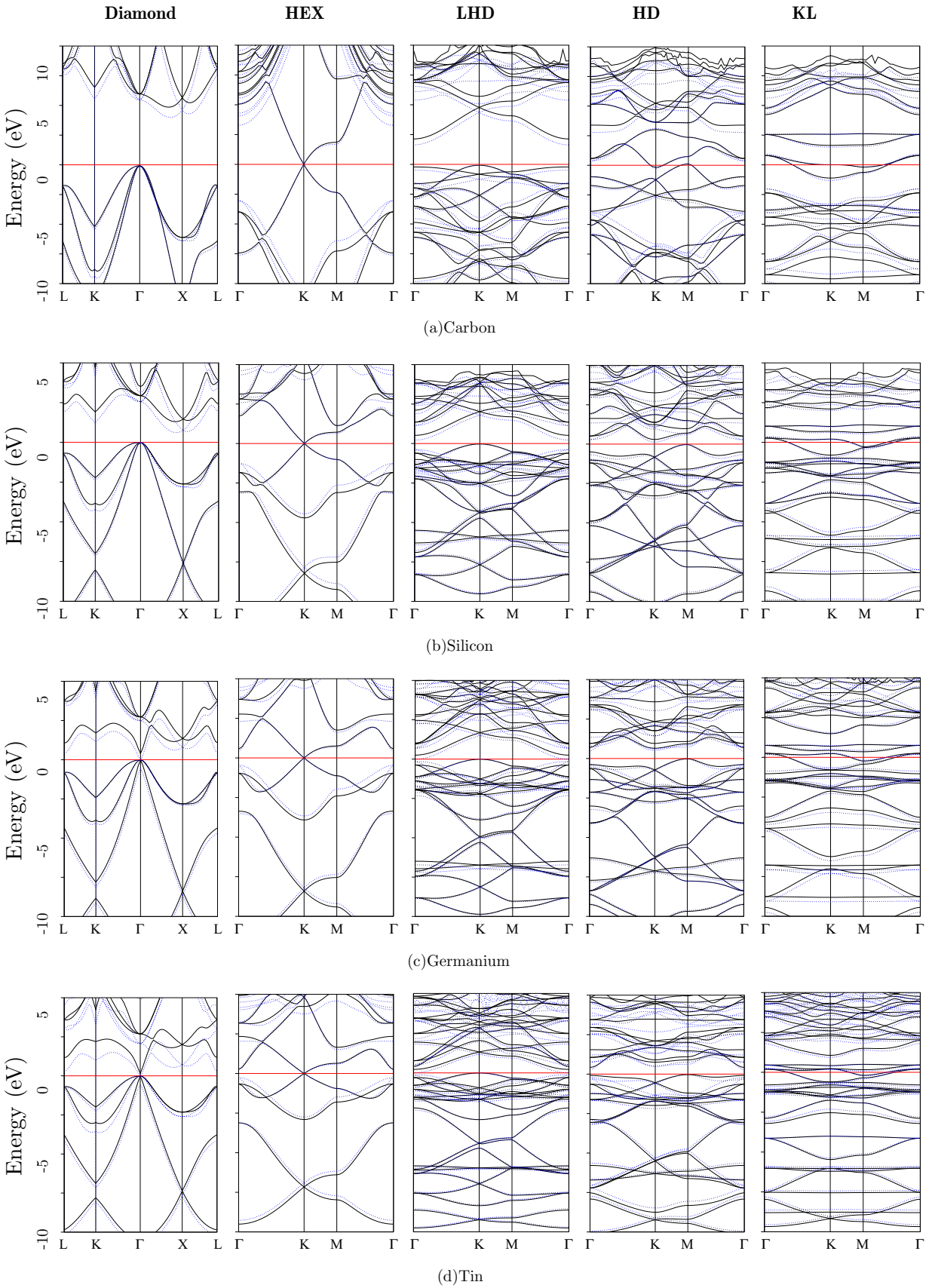

FIG. 3. (Color online) GGA (dotted blue lines) and GGA-1/2 (solid black lines) band structures of carbon, silicon, germanium, and tin for the allotropes diamond, HEX, LHD, HD, and KL. The top of the valence bands or the Fermi level is taken as zero energy (red horizontal lines).

TABLE III. Band gap (in eV) for the 2D allotropes of group-IV materials calculated within GGA, GGA-1/2, and HSE06. CUT parameters (in Bohr radius a_0) obtained for GGA-1/2 calculations are listed in parenthesis. Experimental values are shown for diamond structures. Other theoretical HSE results are given only for diamond.

	Diamond				LHD			HD		
	GGA	GGA-1/2(CUT)	HSE	EXP	GGA	GGA-1/2(CUT)	HSE	GGA	GGA-1/2(CUT)	HSE
C	4.09	4.93(2.36)	5.29[5.76[c]] [60]	5.4 [46]	1.70	2.21(2.68)	2.71	Metal	Metal	Metal
Si	0.62	1.30(3.68)	1.22[1.23[c]] [60]	1.17 [46]	0.25	0.54(4.08)	0.73	0.15	0.32(3.49)	0.43
Ge	0.00	0.41[a][0.86[b]]	0.12[0.74[d]] [59]	0.74 [46]	0.00	0.26[f]	0.36	0.50	0.72[g]	0.79
Sn	0.00	0.00(4.70)	0.00[0.00[e]] [61]	0.00 [46]	0.02	0.23(4.84)	0.32	0.31	0.40(4.29)	0.63

[a]For configuration $+1/4s$-$1/4p$. CUT calculated for s orbital was 2.20 and for p orbital was 4.10.
[b]Same configuration of a but for experimental lattice parameter 5.658 Å.
[c]With HSE03 lattice parameter 3.557 Å for C and 5.454 Å for Si.
[d]With HSE lattice parameter 5.69 Å and 30% of HF mixing.
[e]With HSE06 lattice parameter 6.561 Å.
[f]For configuration $+1/4s$-$1/4p$. CUT calculated for s orbital was 1.70 and for p orbital was 4.30.
[g]For configuration $+1/4s$-$1/4p$. CUT calculated for s orbital was 1.40 and for p orbital was 3.80.

with GGA ones in Fig. 3. While silicon, germanium, and tin are semiconductors for all three phases, carbon presents a metallic behavior in the HD phase. All results in Table III were obtained using GGA lattice constants, which are slightly overestimated as can be seen in Table I.

Regardless, of the underestimation of the band-gap energies within standard DFT (local density approximation or GGA), the resulting values are very similar considering the experimental or the theoretical lattice parameters. For germanium the situation is different. In addition to the band-gap underestimation (GGA predicts a zero gap), the position of the conduction band minimum (CBM) is not described correctly. Experimentally, germanium has a fundamental indirect band gap, $E_g^{\Gamma-L}$, of about 0.74 eV (at $T = 0$ K) [46]. Several calculations predict a direct energy band gap or give the position of the CBM at other high-symmetry points in the BZ than the L point [54–57]. The study of the band structure of germanium is still a challenge, applying the several methods that correct the quasiparticle energy gap [58]. We observe a strong influence of the lattice parameter on the CBM position and the gap value in the diamond structure. By using HSE with GGA theoretical lattice constant we get an unsatisfactory electronic structure, as illustrated in Table III—wrong gap and wrong CBM position. In HSE, the difference between the calculated direct and indirect gap is very small, about 0.01 eV, while measurements predict a difference of 0.15 eV [59]. The GGA-1/2 method suffers from the same difficulties. A gap close to the experimental one can only be reached by considering the experimental lattice parameter and the self-energy of the conduction band. In this case GGA-1/2 predicts an indirect gap of 0.86 eV and a direct gap of 1.02 eV.

In the diamond case the GGA-1/2 method tends to overestimate the indirect gap of Si by about 0.1 eV. The gap of diamond carbon is underestimated by 0.6 eV and the gap of germanium is underestimated by about 0.3 eV. All the HSE gaps are closer to the experimental values (see Table III), except those for germanium. Both 2D dumbbell allotropes in Fig. 3, LHD and HD, represent indirect semiconductors, except for HD carbon, which is a half metal with the electron (hole) pockets at the K (M) points of the BZ. All the band structures of the TD allotropes indicate a metal (not shown in Fig. 3). This fact explains why TD is energetically unfavorable compared to LHD and HD for Si, Ge, and Sn. The indirect gaps of the LHD geometry are given by transitions $K \rightarrow \Gamma$, while for the HD structure of Si, Ge, and Sn, they are given by transitions $M \rightarrow \Gamma$. Only in the Si case the conduction band minimum at K becomes slightly below the Γ minimum, already indicating the possible transition into a half metal for carbon. Our findings for the band structures of 2D dumbbell arrangements are in qualitative agreement with previous studies for Si [25,30] and Sn [31]. Among the six studied 2D allotropes, only the LHD and HD geometries show a semiconducting behavior independent of the group-IV element. The gap opening in the Si-, Ge-, and Sn-derived 2D dumbbell structures LHD and HD is one of the main reasons for their higher cohesive energies, in comparison with their graphenelike sheet crystal modification. Only in the carbon case the extremely strong sp^2 bonds lead to the favorization of the zero-gap semiconductor graphene. The metallic character of the KL allotropes (see Fig. 3) seems to contradict their relative stability, indicated by cohesive energies close or embedded in the LHD and TD values. However, the band structures in Fig. 3 show a pronounced gap within the lowest conduction bands close to the Fermi energy. For adsorbed 2D allotropes one therefore expects that electron transfer from the substrate into the overlayer may stabilize the KL geometry. On the contrary, 2D allotropes with gap (LHD, TD) should be possible to grow within a van der Waals epitaxy, where only almost vanishing charge transfers appear between the overlayer and substrate. We speculate that the zero-gap systems (HEX), graphenelike Si, Ge, and Sn, represent intermediate cases concerning possible charge transfers, which may stabilize the slightly buckled geometries on substrates.

IV. SUMMARY AND CONCLUSIONS

By means of the *ab initio* density functional theory we have studied the atomic geometry and the energetic stability of six 2D allotropes of group-IV elements. Besides the well-known graphenelike sheet crystals silicene, germanene, and stanene, three 2D structures consisting of atomic dumbbells, a MoS_2-like triple atomic layer, and a 2D kagome lattice have

been investigated. The structural optimization shows that all these 2D crystals, despite their different atomic coordination and chemical bonding, give rise to local minima on the total energy surface, i.e., they are at least metastable structures.

In the carbon case we confirm the known result that graphene is the most stable 2D crystal. The pure sp^2 bonding stabilizes such a flat honeycomb geometry of carbon atoms. The situation is totally different for the other group-IV atoms. Already within the MoS_2 geometry the Si, Ge, or Sn atoms gain more energy by chemical bonding than in the frequently discussed graphenelike symmetries silicene, germanene, and stanene. In contrast, the 2D kagome lattice is less stable than the sp^2/sp^3 bonded films. The most energy is gained for 2D dumbbell arrangements of Si and Ge atoms. This especially holds for their honeycomb arrangements. In contrast, also to literature predictions, we found that the triple-layer MoS_2 geometry is most favorable for Sn, not the stanene nor the LHD geometry. The most stable Si-, Ge-, or Sn-based 2D sheet crystals are those with large unit cells and, hence, manifold degrees of freedom due to the many atomic coordinates. The fact that the large honeycomb dumbbell arrangements are the most stable freestanding Si and Ge sheet crystals, as well as the MoS_2 structure for Sn, should help to better understand the various group-IV overlayers with different geometry, translational symmetry, and thickness on metallic and nonmetallic substrates.

The excited electronic states of all the 2D geometries have been investigated taking quasiparticle corrections in an approximate manner into account. Band structures are computed describing exchange and correlation by a hybrid functional or the GGA-1/2 method. For the honeycomb symmetries we found as an important stabilization mechanism the opening of fundamental gaps in the band structure, in contrast to the zero-gap Dirac cone bands in the case of the graphenelike crystals. The 2D honeycomb dumbbell crystals represent indirect semiconductors with gaps of the order of a few tenths of electronvolts. The conduction band minimum is located at the Γ point, whereas the valence band maxima are situated at the BZ boundary at K or M. The small gaps may be interpreted as indications that the LHD and HD dumbbell structures are topological insulators, of course, if spin-orbit interaction is considered, too.

In conclusion, besides complementing the literature, in general, we predicted a tendency for less stability of the slightly buckled graphenelike arrangements of Si, Ge, and Sn atoms; rather, dumbbell geometries are favored. In the Sn case, even the formation of the MoS_2-like triple layers has been predicted to be the most stable 2D geometry. The results have been interpreted in terms of chemical bonding and approximate quasiparticle band structures.

ACKNOWLEDGMENTS

This work was supported by the Brazilian funding agency CAPES, Grants No. 23038.005810/2014-34 and No. 88881.068355/2014-01, and the São Paulo Research Foundation (FAPESP), Grants No. 2012/50738-3 and No. 2014/13907-7.

[1] P. R. Wallace, Phys. Rev. **71**, 622 (1947).
[2] K. S. Novoselov, Science **306**, 666 (2004).
[3] Y. Zhang, Y.-W. Tan, H. L. Stormer, and P. Kim, Nature (London) **438**, 201 (2005).
[4] K. S. Novoselov, A. K. Geim, S. V. Morozov, D. Jiang, M. I. Katsnelson, I. V. Grigorieva, S. V. Dubonos, and A. A. Firsov, Nature (London) **438**, 197 (2005).
[5] C. Berger, Science (Washington, DC, US) **312**, 1191 (2006).
[6] R. R. Nair, P. Blake, A. N. Grigorenko, K. S. Novoselov, T. J. Booth, T. Stauber, N. M. R. Peres, and A. K. Geim, Science (Washington, DC, US) **320**, 1308 (2008).
[7] M. I. Katsnelson, K. S. Novoselov, and A. K. Geim, Nat. Phys. **2**, 620 (2006).
[8] T. Ohta, Science (Washington, DC, US) **313**, 951 (2006).
[9] A. K. Geim and K. S. Novoselov, Nat. Mater. **6**, 183 (2007).
[10] K. S. Novoselov, Z. Jiang, Y. Zhang, S. V. Morozov, H. L. Stormer, U. Zeitler, J. C. Maan, G. S. Boebinger, P. Kim, and A. K. Geim, Science (Washington, DC, US) **315**, 1379 (2007).
[11] A. H. Castro Neto, F. Guinea, N. M. R. Peres, K. S. Novoselov, and A. K. Geim, Rev. Mod. Phys. **81**, 109 (2009).
[12] S. Cahangirov, M. Topsakal, E. Aktürk, H. Sahin, and S. Ciraci, Phys. Rev. Lett. **102**, 236804 (2009).
[13] G. G. Guzmán-Verri and L. C. Lew Yan Voon, Phys. Rev. B **76**, 075131 (2007).
[14] F. Bechstedt, L. Matthes, P. Gori, and O. Pulci, Appl. Phys. Lett. **100**, 261906 (2012).
[15] L. Matthes, P. Gori, O. Pulci, and F. Bechstedt, Phys. Rev. B **87**, 035438 (2013).
[16] L. Matthes, O. Pulci, and F. Bechstedt, J. Phys.: Condens. Matter **25**, 395305 (2013).
[17] Y. Xu, B. Yan, H. J. Zhang, J. Wang, G. Xu, P. Tang, W. Duan, and S. C. Zhang, Phys. Rev. Lett. **111**, 136804 (2013).
[18] B. V. D. Broek, M. Houssa, E. Scalise, G. Pourtois, V. V. Afanasev, and A. Stesmans, 2D Mater. **1**, 021004 (2014).
[19] S. Balendhran, S. Walia, H. Nili, S. Sriram, and M. Bhaskaran, Small **11**, 640 (2015).
[20] P. Vogt, P. De Padova, C. Quaresima, J. Avila, E. Frantzeskakis, M. C. Asensio, A. Resta, B. Ealet, and G. Le Lay, Phys. Rev. Lett. **108**, 155501 (2012).
[21] A. Fleurence, R. Friedlein, T. Ozaki, H. Kawai, Y. Wang, and Y. Yamada-Takamura, Phys. Rev. Lett. **108**, 245501 (2012).
[22] C.-L. Lin, R. Arafune, K. Kawahara, N. Tsukahara, E. Minamitani, Y. Kim, N. Takagi, and M. Kawai, Appl. Phys. Express **5**, 045802 (2012).
[23] M. E. Dávila, L. Xian, S. Cahangirov, A. Rubio, and G. Le Lay, New J. Phys. **16**, 095002 (2014).
[24] E. Bianco, S. Butler, S. Jiang, O. D. Restrepo, W. Windl, and J. E. Goldberger, ACS Nano **7**, 4414 (2013).
[25] V. O. Özçelik and S. Ciraci, J. Phys. Chem. C **117**, 26305 (2013).
[26] D. Kaltsas and L. Tsetseris, Phys. Chem. Chem. Phys. **15**, 9710 (2013).
[27] B. Feng, Z. Ding, S. Meng, Y. Yao, X. He, P. Cheng, L. Chen, and K. Wu, Nano Lett. **12**, 3507 (2012).

[28] A. Resta, T. Leoni, C. Barth, A. Ranguis, C. Becker, T. Bruhn, P. Vogt, and G. Le Lay, Sci. Rep. **3**, 2399 (2013).
[29] L. Chen, C. C. Liu, B. Feng, X. He, P. Cheng, Z. Ding, S. Meng, Y. Yao, and K. Wu, Phys. Rev. Lett. **109**, 056804 (2012).
[30] S. Cahangirov, V. O. Özçelik, L. Xian, J. Avila, S. Cho, M. C. Asensio, S. Ciraci, and A. Rubio, Phys. Rev. B **90**, 035448 (2014).
[31] P. Tang, P. Chen, W. Cao, H. Huang, S. Cahangirov, L. Xian, Y. Xu, S.-C. Zhang, W. Duan, and A. Rubio, Phys. Rev. B **90**, 121408 (2014).
[32] F. Gimbert, C.-C. Lee, R. Friedlein, A. Fleurence, Y. Yamada-Takamura, and T. Ozaki, Phys. Rev. B **90**, 165423 (2014).
[33] Y. Chen, Y. Y. Sun, H. Wang, D. West, Y. Xie, J. Zhong, V. Meunier, M. L. Cohen, and S. B. Zhang, Phys. Rev. Lett. **113**, 085501 (2014).
[34] O. Leenaerts, B. Schoeters, and B. Partoens, Phys. Rev. B **91**, 115202 (2015).
[35] K. Matan, T. Ono, Y. Fukumoto, T. J. Sato, J. Yamaura, M. Yano, K. Morita, and H. Tanaka, Nat. Phys. **6**, 865 (2010).
[36] P. E. Blöchl, Phys. Rev. B **50**, 17953 (1994).
[37] G. Kresse and D. Joubert, Phys. Rev. B **59**, 1758 (1999).
[38] G. Kresse and J. Hafner, Phys. Rev. B **47**, 558 (1993).
[39] G. Kresse and J. Hafner, Phys. Rev. B **49**, 14251 (1994).
[40] G. Kresse and J. Furthmuller, Phys. Rev. B **54**, 11169 (1996).
[41] J. Pack and H. Monkhorst, Phys. Rev. B **13**, 5188 (1976).
[42] F. Bechstedt, *Many-Body Approach to Electronic Excitations*, Springer Series in Solid-State Sciences Vol. 181 (Springer, Berlin, 2015).
[43] W. G. Aulbur, L. Jönsson, and J. W. Wilkins, in *Solid State Physics,* edited by H. Ehrenreich (Academic Press, Orlando, FL, 1999), Vol. 54.
[44] L. G. Ferreira, M. Marques, and L. K. Teles, Phys. Rev. B **78**, 125116 (2008).
[45] L. G. Ferreira, M. Marques, and L. K. Teles, AIP Adv. **1**, 032119 (2011).
[46] C. Kittel, *Introduction to Solid State Physics*, 8th ed. (John Wiley & Sons, Inc., New York, 2011).
[47] J. Heyd, G. E. Scuseria, and M. Ernzerhof, J. Chem. Phys. **118**, 8207 (2003).
[48] J. Heyd, G. E. Scuseria, and M. Ernzerhof, J. Chem. Phys. **124**, 219906 (2006).
[49] M. Mekata, Phys. Today **56**(2), 12 (2003).
[50] N. Masumoto, N. Y. Kim, T. Byrnes, K. Kusudo, A. Löffler, S. Höfling, A. Forchel, and Y. Yamamoto, New J. Phys. **14**, 065002 (2012).
[51] J. Ito, J. Nakamura, and A. Natori, J. Appl. Phys. **103**, 113712 (2008).
[52] A. Al Zahrani, Phys. B (Amsterdam, Neth.) **407**, 992 (2012).
[53] P. Bampoulis, L. Zhang, A. Safaei, R. van Gastel, B. Poelsema, and H. J. W. Zandvliet, J. Phys.: Condens. Matter **26**, 442001 (2014).
[54] A. Fleszar, Phys. Rev. B **64**, 245204 (2001).
[55] W. Ku and A. G. Eguiluz, Phys. Rev. Lett. **89**, 126401 (2002).
[56] M. Rohlfing, P. Krüger, and J. Pollmann, Phys. Rev. B **48**, 17791 (1993).
[57] M. S. Hybertsen and S. G. Louie, Phys. Rev. B **34**, 5390 (1986).
[58] C. Ekuma, M. Jarrell, J. Moreno, and D. Bagayoko, Phys. Lett. A **377**, 2172 (2013).
[59] J. R. Weber, A. Janotti, and C. G. Van de Walle, Phys. Rev. B **87**, 035203 (2013).
[60] J. Paier, M. Marsman, K. Hummer, G. Kresse, I. C. Gerber, and J. G. Angyan, J. Chem. Phys. **124**, 154709 (2006).
[61] K. Hummer, J. Harl, and G. Kresse, Phys. Rev. B **80**, 115205 (2009).